

Bistatic ISAR Sparse Aperture Maneuvering Target Translational Compensation Imaging Algorithm

Hanshen ZHU, Wenhua HU, Baofeng GUO, Xiaoxiu ZHU, Dongfang XUE, Chang'an ZHU

Dept. of Electronic and Optical Engineering, Shijiazhuang Campus of Army Engineering University,
Heping Street 97, 050003, Shijiazhuang, China

352399814@qq.com, hwhsaq@sina.com, 15132497492@126.com, {zhuxiaoxiu13,dongfang_25}@163.com

Submitted January 1, 2022 / Accepted May 31, 2022 / Online first June 22, 2022

Abstract. For bistatic inverse synthetic aperture radar (Bi-ISAR), the non-uniform motion state of maneuvering target and the time-varying bistatic angle make the traditional imaging method of moving target face the problem of translation compensation, and the traditional translation compensation method is not suitable for the return wave in the case of sparse aperture. In this paper, a compensation imaging method combining two-dimension joint linearized Bregman iteration and image contrast search is proposed. The translation compensation problem can be transformed into two-dimension joint compressed sensing sparse reconstruction and moving target motion parameter estimation. The proposed algorithm makes use of the gain of echo two-dimension compression, greatly improves the accuracy of translation compensation and the quality of target image and has stronger robustness to noise. The processing results of simulation data verify the effectiveness and superiority of the algorithm.

Keywords

Bistatic-ISAR, maneuvering target, sparse aperture, translational compensation

1. Introduction

Inverse synthetic aperture radar (ISAR) can generate fine two-dimension reflectivity images of the observed target and plays an important role in target tracking and recognition. Compared with traditional monostatic ISAR imaging, bistatic ISAR (Bi-ISAR) (or multistatic ISAR) imaging adopts the transmitter-receiver separation mode, which enhances the flexibility of the system and improves the probability of imaging. It has attracted the attention of many scholars [1] and has become a hot topic in the research of modern radar technology.

At present, many sparse aperture imaging algorithms with high operation efficiency and excellent imaging quality have been proposed, including linear prediction [2], [3], modern spectrum estimation [4–6], and sparse signal reconstruction [7–12]. Among the three methods, sparse

signal reconstruction based on compressed sensing theory [13] has the best imaging effect and the fastest speed and has attracted extensive attention. However, the models established with previous methods to solve the imaging problem are based on the assumption that the translation compensation has been completed. Translation compensation for the echo in the case of sparse aperture was ignored. The time variation of the maneuvering component and bistatic angle of the maneuvering target will lead to the time variation of the target Doppler frequency, and the traditional translation compensation method is not suitable for the echo in the case of sparse aperture. Therefore, it is necessary to find a simple and efficient algorithm with ideal imaging performance to solve the above problems.

In this paper, a method combining two-dimension joint linearized Bregman iteration (2D-JLBI) and image contrast (IC) search is proposed. The quadratic polynomial is used to fit the trajectory of the maneuvering target. The Bi-ISAR sparse aperture maneuvering target echo signal model with translation error term is established. The phase compensation term is established with the rough motion information obtained by narrowband velocity measurement. The image is reconstructed by the 2D-JLBI algorithm, and the compensation term is updated based on the translation trajectory parameters corresponding to the IC search optimal image. In this way, high-quality images can be obtained.

2. Relative Work

At present, sparse aperture signal reconstruction by compressed sensing technology can be divided into two categories. The first is the processing of the range direction and azimuth direction separately. Although this method has fast speed and excellent performance, it destroys the coupling of range and azimuth dimension and degrades the imaging performance [14]. The second is the processing of range azimuth coupling. The reconstruction of the two-dimension coupled echo matrix is mainly conducted with the following methods. The first is row by row and column by column processing. Because the row by row and column processing method not only includes a large number

of redundant calculations, the calculation efficiency is low, but also destroys the correlation between row and column data, and the reconstruction effect is not as good as block processing, so few people use this calculation method in recent years [15]. The second is vectorization processing. A two-dimensional pattern-coupled sparse Bayesian learning (2D-PCSBL) algorithm for ISAR imaging is proposed in [16]. It utilizes a parameter to characterize the pattern relevance between a coefficient and its four neighboring coefficients of the adjacent rows and columns in the two-dimensional data matrix. The model used can provide flexibility to model any block-sparse structure signals and has a good performance for ISAR imaging. However, the memory storage space and the computational complexity are high due to the vectorized solution. When the imaging scene is highly complex, the amount of calculation is large and the real-time performance is poor. The third is block processing, and this is a processing method of re-fusion imaging after block by block processing. In order to reduce the high computational complexity and memory storage space caused by the whole matrix vectorization, the observation scene of [17] is segmented into multiple sub-scenes and each sub-scene data is reconstructed by the MB-PCSBL method respectively. And then the whole fusion image is obtained through the stitching of the sub-scenes fusion imaging results. This method can indeed shorten the calculation time, but it also sacrifices part of the imaging performance. The fourth method combines two-dimension sparse reconstruction algorithms for reconstruction, such as the two-dimension fast iterative shrinkage-thresholding algorithm (2D-FISTA) and two-dimension smooth l_0 norm reconstruction algorithm (2D-SL0). However, these two algorithms have poor performance under the condition of low SNR [18].

To sum up, previous algorithms have various shortcomings. The contributions of this paper are as follows:

- The translation compensation is transformed into compressed sensing two-dimension joint sparse reconstruction and maneuvering target motion parameter estimation, which not only makes full use of the gain of echo two-dimension compression but also reduces vectorization calculation and row by row and column processing.
- Through the combination of 2D-JLBI and IC search, compensation and high-quality imaging can be completed under different aperture missing conditions and high aperture missing rates.
- Compared with other two-dimension joint sparse reconstruction algorithms, the algorithm proposed in this paper contributes to the highest image quality, which is manifested in the maximum contrast, the lowest entropy, and stronger robustness to noise.

3. Modeling of Bi-ISAR Sparse Aperture Maneuvering Target Echo Signal

The Bi-ISAR imaging geometric model is shown in Fig. 1 [1]. Tr is the transmitting station, Re is the receiving station, L is the radar baseline length, and E is the equivalent monostatic radar position. It is supposed that the target is maneuvering in space, with the velocity of v and the acceleration of a . At the imaging start time t_0 , the target centroid is O and the bistatic angle is β_0 . With the target centroid as the origin and the bisector y of the bistatic angle as the axis, a right-hand coordinate system xOy is established. In this coordinate system, the coordinate of the scattering point P is (x_p, y_p) , the length of OP is d and the included angle with the x axis is α_0 . At the time t_p , the target centroid translates to the O_p point. The coordinate system $x'O_py'$ is obtained after the translation of the coordinate system xOy , where O_p located. The bisector of the bistatic angle is the v axis, and the right-hand coordinate system $uO_p v$ is established. In this coordinate system, the coordinate of scattering point P is recorded as $P_m(x_{p_m}, y_{p_m})$, the included angle between $O_p P$ and u axis is α_m , and the angle of equivalent monostatic radar is θ_m .

It is assumed that Bi-ISAR transmits LFM signal, and its mathematical expression is as follows:

$$s(\hat{t}, t_m) = A \text{rect}\left(\frac{\hat{t}}{T_p}\right) \exp\left[j2\pi\left(f_c \hat{t} + \frac{1}{2} \mu \hat{t}^2\right)\right] \quad (1)$$

where A represents the backscattering amplitude, $\text{rect}(\cdot)$ represents rectangular window function and

$$\text{rect}(u) = \begin{cases} 1 & (|u| \leq 0.5) \\ 0 & (|u| > 0.5) \end{cases}, \quad t \text{ represents full time, } PRT$$

represents pulse repetition time, $t_m = m PRT$ represents slow time, $\hat{t} = t - m PRT$ represents fast time and $m = [1:M]$, M is the total number of pulses, T_p is the pulse width, f_c is the carrier frequency, and μ is the chirp rate, where $\mu = B/T_p$.

The obtained target echo signal is down-converted to fundamental frequency echo, as shown below:

$$s(\hat{t}, t_m) = \sum_{k=1}^K \sigma_k a\left(\hat{t} - \frac{R_k(t_m)}{c}, t_m\right) \exp\left(-j2\pi f_c \frac{R_k(t_m)}{c}\right) \quad (2)$$

where K is the number of scattering points, σ_k is the backscattering coefficient corresponding to the K -th scattering point, $a(\cdot)$ represents the complex envelope of the signal, $R_k(t_m)$ represents the sum of the distance from the K -th scattering point to the transceiver at a slow time t_m (echo signal analysis adopts the “go-stop” hypothesis [19]), and c is the propagation speed of the electro-magnetic wave.

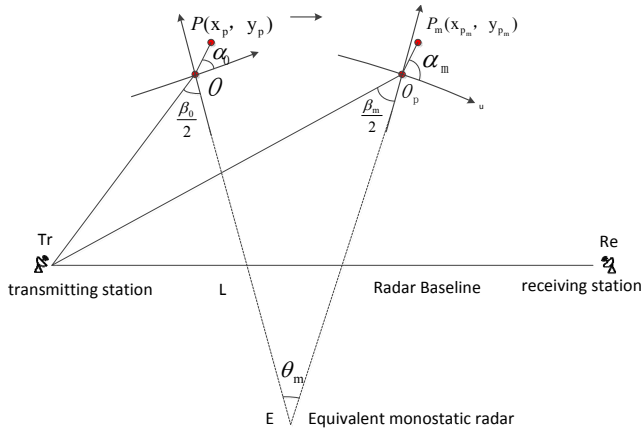


Fig. 1. Bi-ISAR imaging geometric model.

$$R_k(t_m) = R_r(t_m) + 2(x_k \sin \theta_m + y_k \cos \theta_m) \cos \frac{\beta_m}{2} \quad (3)$$

where \$R_r(t_m)\$ represents the instantaneous distance from the rotation center of the maneuvering target to the transceiver at \$t_m\$, \$\beta_m\$ corresponds to the bistatic angle at \$t_m\$, \$2(x_k \sin \theta_m + y_k \cos \theta_m) \cos \frac{\beta_m}{2}\$ represents the distance change caused by target rotation.

\$S_r(f, t_m)\$ can be obtained by transforming \$s(t, t_m)\$ from fast time domain to baseband frequency domain,

$$S_r(f, t_m) = \sum_{k=1}^K \sigma'_k A(f) \exp \left[-j2\pi \frac{R_k(t_m)}{c} (f + f_c) \right] \quad (4)$$

where \$A(f)\$ is the Fourier transform of \$a \left(\hat{i} - \frac{R_k(t_m)}{c}, t_m \right)\$.

By performing matched filtering on (5) and ignoring the imaging independent term, it can be obtained that the signal in azimuth time and distance frequency domain is:

$$\begin{aligned} S_r(f, t_m) &= \sum_{k=1}^K \sigma'_k \exp \left[-j2\pi \frac{R_k(t_m)}{c} (f + f_c) \right] \\ &= \sum_{k=1}^K \sigma'_k \exp \left[-j2\pi \frac{R_r(t_m)}{c} (f + f_c) \right] \cdot \\ &\exp \left[-j4\pi \frac{x_k \sin \theta_m + y_k \cos \theta_m}{c} (f + f_c) \cos \frac{\beta_m}{2} \right]. \end{aligned} \quad (5)$$

Generally speaking, Bi-ISAR imaging accumulation time should be short. During this time, it can be considered that the target rotates uniformly during the observation and the rotation angle is small. The following approximation can be made: \$\sin \theta_m \approx \omega t_m + \frac{1}{2} \omega_a t_m^2\$, \$\cos \theta_m \approx 1\$. In addition, it is assumed that the bistatic angle \$\beta(t_m)\$ is constant \$\beta\$ during the imaging.

Therefore, the backscattered signal of (5) can be written as:

$$\begin{aligned} S_r(f, t_m) &= \exp \left[-j2\pi \frac{R_r(t_m)}{c} (f + f_c) \right] \cdot \\ &\left[\sum_{k=1}^K \sigma'_k \exp \left(-j4\pi \frac{x_k \omega t_m + \frac{1}{2} x_k \omega_a t_m^2 + y_k}{c} (f + f_c) \cos \frac{\beta}{2} \right) \right]. \end{aligned} \quad (6)$$

After the discretization of (6), equation (7) is obtained

$$\begin{aligned} s(n, p) &= \exp \left[-j2\pi \frac{R_r(t_m)}{c} (f_r + f_c) \right] \cdot \sum_{p=1}^P \sum_{q=1}^Q \sigma(x_p, y_q) \\ &\exp \left[-j\frac{4\pi}{c} \left(x_p \omega t_n + \frac{1}{2} x_p \omega_a t_n^2 + y_q \right) (f_r + f_c) \cos \frac{\beta}{2} \right]. \end{aligned} \quad (7)$$

\$P, Q\$ represent the index of the discrete backscattering point. Next, each phase term in (7) is analyzed as follows:

\$\exp \left[-j2\pi \frac{R_r(t_m)}{c} (f_c + f_r) \right]\$ represents the influence of target translation component on echo envelope. In the second phase term, \$\exp \left[-j\frac{4\pi}{c} y_q f_c \cos \frac{\beta}{2} \right]\$ does not change with azimuth time and range frequency, and can be regarded as a constant term; \$\exp \left[-j\frac{4\pi}{c} x_p \omega t_n f_r \cos \frac{\beta}{2} \right]\$ and \$\exp \left[-j\frac{2\pi}{c} x_p \omega_a t_n^2 f_r \cos \frac{\beta}{2} \right]\$ are negligible in small angle imaging. Therefore, equation (7) can be expressed as follows:

$$\begin{aligned} s(n, p) &= \exp \left[-j2\pi \frac{R_r(t_m)}{c} (f_c + f_r) \right] \\ &\sum_{p=1}^P \sum_{q=1}^Q \sigma(x_p, y_q) \exp \left(-j2\pi \left(1 + \frac{\gamma t_n}{2} \right) f_p t_n \cos \frac{\beta}{2} \right) \\ &\exp \left(-j\frac{4\pi}{c} y_q f_r \cos \frac{\beta}{2} \right). \end{aligned} \quad (8)$$

Among the parameters in (8), \$\gamma = \omega_a/\omega\$ only depends on the target rotation parameters and is the same for all scattering points. \$f_p = [1:N] \times \Delta f_d\$, where \$N\$ is sampling points, \$\Delta f_d\$ is the Doppler resolution. In this paper, the method of Li et al. [7] was used to estimate the parameter \$\gamma\$. The echo was integrated with the fast time, and the two-dimension echo signal was transformed into a column of azimuth signals. And then \$\gamma\$ was reconstructed using the smoothing norm \$l_0\$. The proximity between \$\gamma\$ and \$\omega_a/\omega\$ was judged by entropy, and the value with the smallest entropy was taken as the \$\gamma\$ estimation \$\hat{\gamma}\$.

It can be seen from (8) that there is a Fourier transform pair relationship between the range coordinate and the range frequency of the target, and there is a matching Fourier transform pair relationship between the azimuth

coordinate and the azimuth dimension time with parameter γ . Considering the random sparsity of the azimuth, the target maneuver, and the observation noise, the relationship between the echo signal, translation error and the imaging scene can be expressed in the form of matrix [20]:

$$\mathbf{S} = \mathbf{E} \odot (\mathbf{A}\mathbf{X}\mathbf{B}) + \mathbf{N}_o \quad (9)$$

where \odot represents Hadamard product, and $\mathbf{S} \in \mathbb{C}^{N \times R}$ represents echo signal matrix in range frequency and azimuth time domain; $\mathbf{E} \in \mathbb{C}^{N \times R}$ represents the envelope walk and phase shift caused by the translational component of the target to the echo, and $E_{nr} = \exp\left[-j2\pi \frac{R_r(n)}{c} (f_c + f_r)\right]$.

In the case of azimuth random sparsity, $\mathbf{A} \in \mathbb{C}^{N \times M}$ represents the matching Fourier transform matrix with parameter γ in the azimuth dimension; $\mathbf{B} \in \mathbb{C}^{R \times R}$ represents the Fourier transform matrix in the distance dimension; $\mathbf{X} \in \mathbb{C}^{M \times R}$ represents the discrete imaging scene; $\mathbf{N}_o \in \mathbb{C}^{N \times R}$ represents observation noise. N , M and R respectively represent the number of azimuthal sampling pulses, the number of scene azimuthal units and the number of echo range dimension samples.

Due to the maneuverability of the target, the translation error term of the target usually has a high-order term varying with slow time. In order to establish the compensation term, this paper uses quadratic polynomial to fit the motion trajectory of the target along the baseline direction of the bistatic radar. It is assumed that the target has the following motion state:

$$d = \sum_{k=0}^2 a_k t_n^k \quad (10)$$

With this model and the sparsity of the Bi-ISAR imaging scene, the translation error correction problem of the Bi-ISAR target is transformed into an optimization problem as follows:

$$\{\hat{\mathbf{X}}, \hat{\mathbf{a}}\} = \arg \min_{\mathbf{X}, \mathbf{a}} \left\{ \|\mathbf{S} - \mathbf{E}(\mathbf{a}) \odot (\mathbf{A}\mathbf{X}\mathbf{B})\|_F^2 + \lambda \|\mathbf{X}\|_1 \right\} \quad (11)$$

where $\|\cdot\|_F$ represents the norm of Frobenius matrix, $\|\cdot\|_1$ represents the l_1 norm of the matrix, \mathbf{a} is the vector composed of motion trajectory fitting polynomial coefficients, and λ represents the regularization parameter of sparse term, which is used to control the estimation accuracy.

4. Algorithm Solving

Next, the optimization problem of (11) is solved by alternately updating the imaging scene \mathbf{X} and the polynomial coefficient \mathbf{a} .

4.1 Imaging Scene Updating

The first step of the algorithm is to update the imag-

ing scene \mathbf{X} , namely, equation (11), without considering the influence of translational polynomial parameters. The corresponding optimization problem is in the following form:

$$\begin{aligned} \hat{\mathbf{X}}^{(t+1)} &= \arg \min_{\mathbf{X}} \left\{ \|\mathbf{S} - \mathbf{E}(\hat{\mathbf{a}}^{(t)}) \odot (\mathbf{A}\mathbf{X}\mathbf{B})\|_F^2 + \lambda \|\mathbf{X}\|_1 \right\} \\ &= \arg \min_{\mathbf{X}} \left\{ \|\mathbf{S} \odot \mathbf{E}(\hat{\mathbf{a}}^{(t)})^* - (\mathbf{A}\mathbf{X}\mathbf{B})\|_F^2 + \lambda \|\mathbf{X}\|_1 \right\}. \end{aligned} \quad (12)$$

According to literature [20], during “residual back substitution”, the stagnation step of each iteration is estimated by the “kicking” method. The weight parameter η is adjusted, the weight between the residual and the measured value is controlled, and the condition number of the perception matrix is reduced. The algorithm is improved in the above three ways to greatly reduce the number of iterations. The iterative format of the improved 2D-JLBI algorithm (12) is given as follows:

$$\begin{cases} \mathbf{R}^{(k)} = \mathbf{S}^{(k)} - \mathbf{A}\mathbf{X}^{(k)}\mathbf{B}, \\ \mathbf{V}^{(k+1)} = \mathbf{V}^{(k)} + \mathbf{A}^* \mathbf{R}^{(k)} \mathbf{B}^*, \\ \mathbf{X}^{(k+1)} = \delta \text{csoft}_{\mu} \left[\mathbf{V}^{(k+1)} \right], \\ \mathbf{S}^{(k+1)} = \mathbf{S} + \eta \mathbf{R}^{(k)}. \end{cases} \quad (13)$$

$\mathbf{R}^{(k)}$ represents the residual of each iteration; $\mathbf{X}^{(k+1)}$ is the result of each iteration; $\mathbf{V}^{(k+1)}$ is the intermediate variable; $\mathbf{X}^{(0)} = \mathbf{V}^{(0)} = \mathbf{0}$; $\mathbf{A}^* = \mathbf{A}^H (\mathbf{A}\mathbf{A}^H)^{-1}$; $\mathbf{B}^* = (\mathbf{B}^H \mathbf{B})^{-1} \mathbf{B}^H$. The parameter selection method of the algorithm is described in the study of Zhu et al. [21] and will not be detailed here.

Then the above methods are used to optimize the imaging scene. The flow chart of the algorithm is shown in Tab. 1.

Input: Matrices \mathbf{A} , \mathbf{B} and $\mathbf{Y} = \mathbf{s} \odot \{\mathbf{E}[\hat{\mathbf{a}}(t)]\}^*$, Maximum number of iterations k_{\max} , parameter μ
Initialization: Select appropriate parameters δ and η , initialize $\mathbf{X}^{(0)} = \mathbf{V}^{(0)} = \mathbf{0}$.
Cyclic iterative solution: For $k = 0: k_{\max}$ <ol style="list-style-type: none"> 1. Update residual $\mathbf{R}^{(k)}$; 2. Update intermediate variables $\mathbf{V}^{(k+1)}$; 3. Update imaging scene $\mathbf{X}^{(k+1)}$; 4. Update $\mathbf{Y}^{(k+1)}$; 5. Judge whether the algorithm converges. If it converges, it will jump out of the loop.
End
Output: final scene estimate $\hat{\mathbf{X}}^{(k+1)} = \mathbf{X}^{(k)}$

Tab. 1. 2D-JLBI reconstructed image process.

4.2 Polynomial Coefficient Updating

It can be seen from the previous section that the quality of the reconstructed image mainly depends on the construction of the phase compensation term, and the accuracy of the phase compensation term depends on the estimation of translational trajectory parameters. In other words, the accuracy of translational trajectory parameters directly

affects the final imaging effect, and image optimization can finally be transformed into maneuvering target motion parameter estimation. The second step of the algorithm is to update the translation polynomial coefficient a . When the imaging scene has been optimized, the form of the optimization problem corresponding to (11) is transformed as follows:

$$\hat{\mathbf{a}}^{(t+1)} = \arg \min_a \left\{ \left\| \mathbf{S} - \mathbf{E}(a) \odot \left[\mathbf{A} \mathbf{X}^{(t+1)} \mathbf{B} \right] \right\|_F^2 \right\}. \quad (14)$$

The analytical solution for this optimization problem cannot be obtained. In this section, the estimated value $\hat{\mathbf{a}}$ of translational trajectory parameters is updated based on IC search.

In order to accurately measure the imaging quality, IC search is introduced, which is defined as the ratio of the standard deviation of image amplitude ISAR(\hat{t}, \hat{f}_d) to the average value:

$$IC = \frac{\sqrt{A \left\{ \left[\text{ISAR}(\hat{t}, \hat{f}_d) \right] - A \left[\text{ISAR}(\hat{t}, \hat{f}_d) \right] \right\}^2}}{A \left[\text{ISAR}(\hat{t}, \hat{f}_d) \right]} \quad (15)$$

where ISAR(\hat{t}, \hat{f}_d) is the complex amplitude of the image and A(.) is the mean operation. In the established scattering point model, the larger the IC, the larger the amplitude value at the k -th scattering point than the image mean, and the higher the image quality and the focusing degree. When IC is small, the amplitude value at the k -th scattering point is close to the image mean, and the image is blurred and the focusing degree is low. Therefore, IC can be used to evaluate the imaging quality.

In order to obtain accurate motion information of the maneuvering target and establish the compensation term, the rough target speed information is obtained and taken as the initial value. Bi-ISAR usually alternatively uses wide-band and narrow-band signals as the transmission signal. While transmitting the wide-band signal to determine the nature of the target, improve the information perception and identify the classified target, the radar is also transmitting the narrow-band signal. The range information of the target is obtained by transmitting the narrow-band signal, and the preliminary estimation of the speed of the target can be obtained by the curve fitting of the range information. However, due to the poor range resolution of the narrow-band signal, the accuracy of the obtained velocity information is not very high, and it is necessary to further accurately estimate the velocity parameters. In this paper, the parameters of the motion trajectory are updated and the reconstructed image is obtained. It is assumed that the rough velocity information obtained by the narrowband signal is a_0 , and the specific updating process is shown in Tab. 2.

With the combination of Tab. 1 and Tab. 2, the flow of the overall algorithm is obtained, as shown in Fig. 2.

Input: Initial value of motion parameter a_0 .
Initialization: Select the appropriate search range θ and step α to initialize the contrast matrix $\psi = 0$.
Solve based on IC search:
For
1. Taking the initial value a_0 as the center and θ as the search range, the search starting point $\bar{a}_0 = a_0 - \theta/2$ is obtained;
2. Generate compensation matrix $\mathbf{E}(\bar{a}_0)$;
3. Update imaging scene \mathbf{X} ;
4. Calculate the contrast of scene \mathbf{X} and store it in ψ ;
5. Update $a = a + \alpha$.
6. Whether a is within the search scope, if not, jump out of the loop.
End
7. Index P corresponding to the maximum value of ψ in the calculation.
8. Output the image $\hat{\mathbf{X}}$ corresponding to $\hat{\mathbf{a}}$ corresponding to P .
Output: Motion parameter update value $\hat{\mathbf{a}}$; Image estimate $\hat{\mathbf{X}}$.

Tab. 2. The updating process of the motion parameter a .

5. Simulation Results

The simulation experiment environment in this paper is Windows 10 64-bit operating system, Matlab R2018b software platform. The main parameters of the computer used in the simulation are as follows: the processor is Intel Core i7-6700HQ, the main frequency is 2.60 GHz and the memory is 16.0 GB. In this section, the performance of the proposed algorithm is verified from the aspects of aperture missing and echo SNR by experimental simulation. In order to explain the advantages of the algorithm, target to background ratio (TBR) and image entropy E_n are used as the measurement standards. They are shown in (16).

$$\begin{cases} TBR = 10 \lg 10 \left[\frac{\sum_{(m,n \in T)} |A(m,n)|^2}{\sum_{(m,n \in B)} |A(m,n)|^2} \right], \\ E_n = - \sum_{m=1}^M \sum_{n=1}^N p(m,n) \ln p(m,n) \end{cases} \quad (16)$$

where \mathbf{T} and \mathbf{B} respectively represent signals in the target area and signals outside the target area, \mathbf{A} represents target image, and

$$p(m,n) = \frac{|A(m,n)|}{\sum_{m=1}^M \sum_{n=1}^N |A(m,n)|} \quad (17)$$

TBR is the ratio of signal intensity in the target region to signal intensity outside the target region and it can effectively characterize the SNR of imaging and evaluate the estimation accuracy and noise suppression performance of imaging. The larger the value, the better is the accuracy and the performance. Image entropy E_n is used to reflect the average amount of information in the image, and can evaluate the overall quality of the target image. The brighter the value, the better is the quality. The simulation scene of the Bi-ISAR sparse aperture maneuvering target is

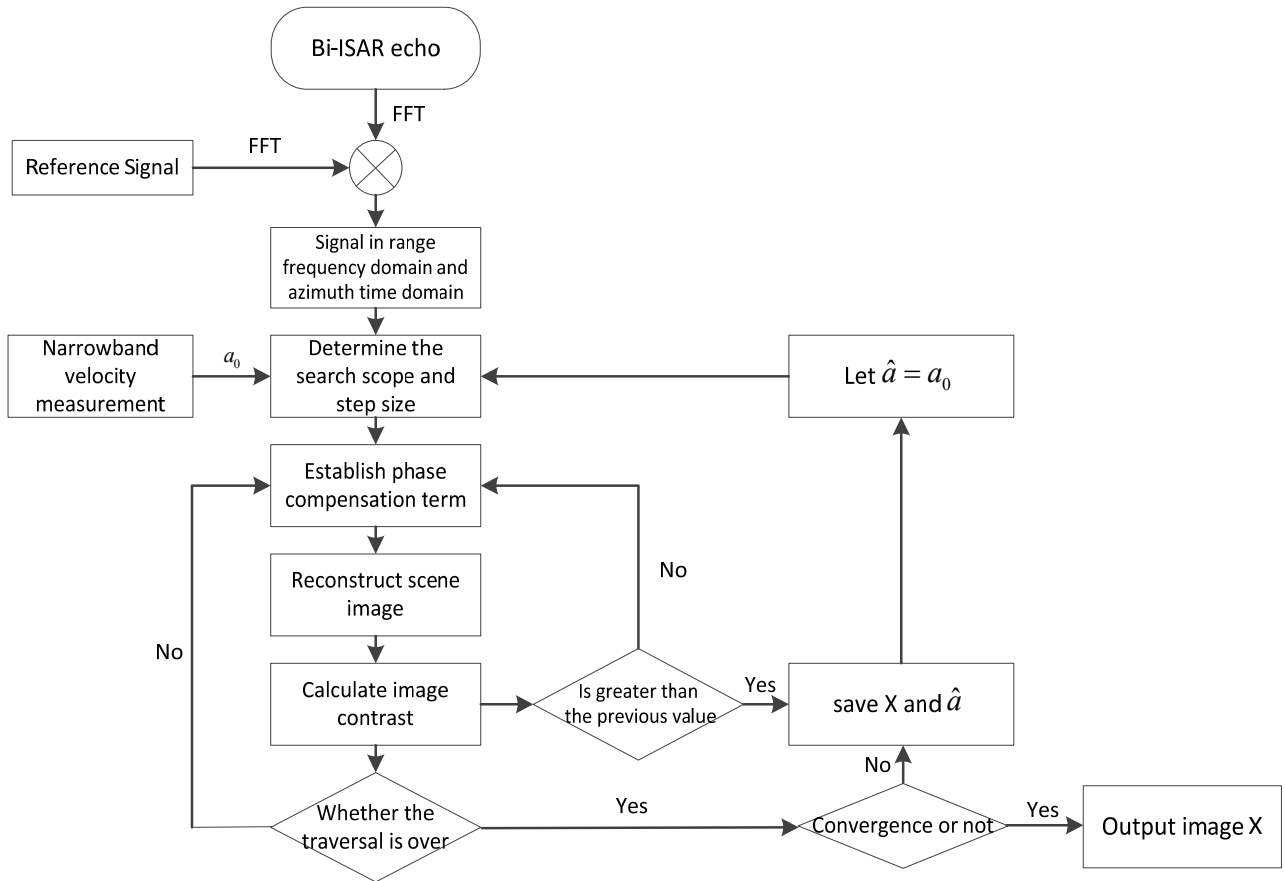
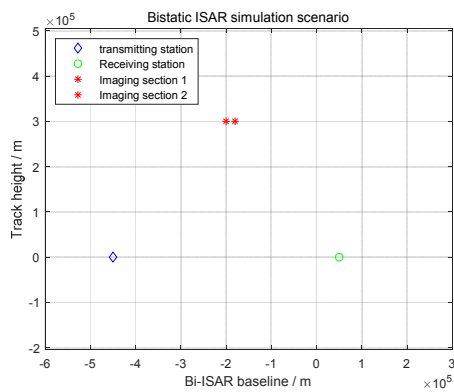
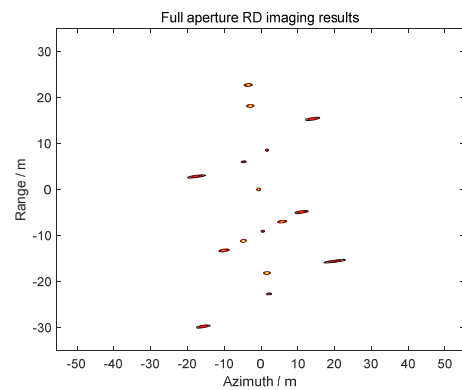


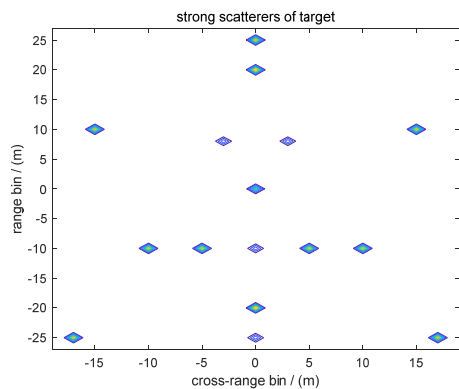
Fig. 2. Bi-ISAR sparse aperture maneuvering target translation compensation imaging algorithm flow.



(a) Bi-ISAR simulation scenario.



(c) Full aperture RD imaging results.



(b) Strong scattering point model.

Fig. 3. Simulation experiment environment.

Parameters	Value	Parameters	Value
Carrier Frequency	10 GHz	Pulse Repetition Time	0.02 s
Bandwidth	50 MHz	Pulse Width	50 Hz
Sampling Rate	6.25 GHz	Range Resolution	0.2838 m
Imaging Time	6 s	Azimuth Resolution	0.4634 m

Tab. 3. Simulation experiment parameters.

shown in Fig. 3(a), the target scattering point model is shown in Fig. 3(b), the full aperture Range-Doppler imaging results are shown in Fig. 3(c), and parameter settings for the simulation are shown in Tab. 3. It is assumed that the baseline length of the two bases is 500 km, and the

target is accelerating uniformly from the median range of the transceiver radar to the receiving radar at an altitude of 300 km at a speed of $v_0 = 3000$ m/s and $a_0 = 100$ m/s². The median range of the transceiver radar was taken as the imaging starting point, and 300 pulses were intercepted as imaging data. The cumulative angle of the observation time was 2.0°, and the variation range of the double base angle was (79.49°, 79.61°), which met the condition that the target rotation angle was small during the observation.

5.1 Performance Verification of the Algorithm in Different Cases of Aperture Missing

In the case of sparse aperture, by changing the missing aperture, the imaging results of the algorithm proposed

in this paper, 2D-SL0 search algorithm based on contrast search and 2D-FISTA search algorithm based on contrast search, are compared to verify the effectiveness and superiority of the algorithm in this study. This comparison was conducted when the SNR is 10 dB, the echo signal is randomly missing (random sparse aperture) and block missing (block sparse aperture), and the missing rate is different. Figure 4 lists the imaging results when the signal is 50% random missing, 50% block missing, 75% random missing and 75% block missing, respectively. Figures 4(a)–4(c) show the imaging results of the three algorithms when the signal is 50% random missing; Figures 4(d)–4(f) show the imaging results when the signal is 75% random missing; Figures 4(g)–4(i) show the imaging results under the condition of the signal is 50% block missing. Figures 4(j)–4(l) show the results when the signal is 75% block missing. The imaging indicators are shown in Tab. 4.

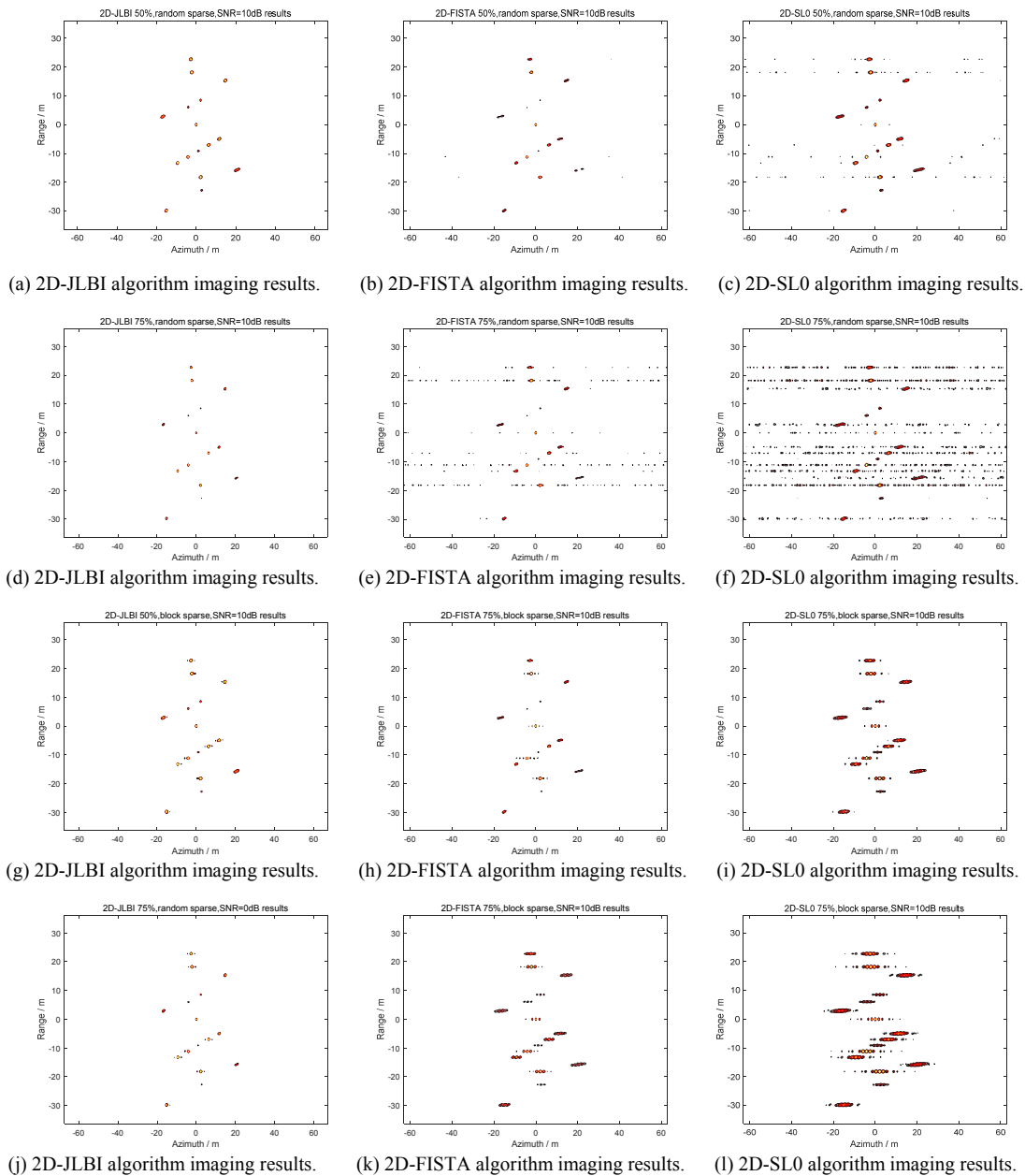


Fig. 4. Imaging results of three algorithms under different aperture missing conditions.

		50% random missing	75% random missing	50% block missing	75% block missing
Image Entropy	2D-JLBI	4.5139	8.5268	6.2066	12.2537
	2D-FISTA	8.0082	11.1453	7.7779	13.7174
	2D-SL0	11.0669	15.6461	13.6040	18.2587
TBR	2D-JLBI	40.0454	25.9917	11.1038	8.1794
	2D-FISTA	17.7582	8.5203	9.4103	6.4295
	2D-SL0	5.8646	3.6388	4.1963	2.1167

Tab. 4. Comparison of algorithm imaging indexes under different aperture missing conditions.

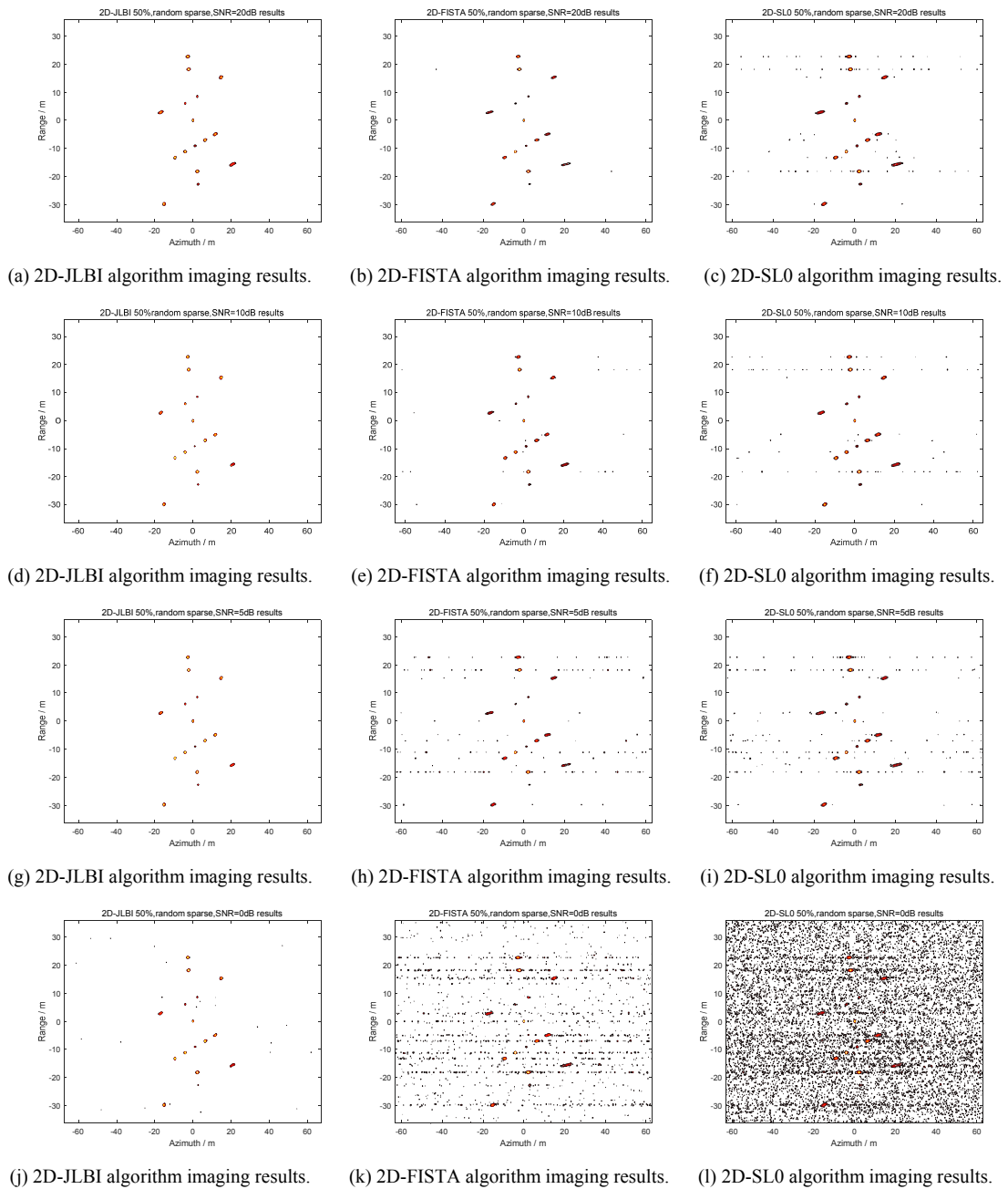


Fig. 5. Imaging results of three algorithms under different SNR conditions.

	SNR	20dB	10dB	5dB	0dB
Image Entropy	2D-JLBI	4.4144	4.5139	5.1207	7.6618
	2D-FISTA	7.1084	8.0082	13.3525	20.2645
	2D-SL0	10.8522	11.0669	15.2654	40.3256
TBR	2D-JLBI	43.6584	40.0454	36.4667	31.6584
	2D-FISTA	23.2455	17.7582	10.5463	2.0299
	2D-SL0	5.5605	5.8646	4.1654	0.2342

Tab. 5. Comparison of algorithm imaging indexes under different SNR conditions.

Figure 4 shows that when the missing rate is 50%, whether random or block missing, the algorithm proposed in this paper can complete compensation and reconstruction of images perfectly. The 2D-FISTA algorithm and 2D-SL0 algorithm can restore an outline of the general target, but there are many false scattering points and the defocusing phenomenon is serious, and the noise suppression effect is poor. It is indicated that the reconstruction performance of the proposed algorithm is better than that of the other two algorithms at the same data missing rate, especially when the missing rate reaches 75%. Under this situation, the imaging quality of the other two algorithms decreases rapidly, and the defocus of scattering points becomes serious, with more false scattering points and worse anti-noise performance. In the random missing case, scattering points in the imaging results of the 2D-SL0 algorithm are almost drowned by noise. In the block missing case, the defocusing of the latter two algorithms is very serious, but the algorithm in this paper can complete compensation and high-quality imaging, indicating that the algorithm in this paper can still achieve high-quality imaging even with a lot of missing data. It can also be seen from Tab. 4 that under the same data missing condition, the image entropy value generated by the algorithm in this paper is the smallest, and its TBR value is the largest, followed by that of the 2D-FISTA algorithm and the 2D-SL0 algorithm. The smaller the data missing rate, the better the reconstruction effect. In the case of the same data miss rate, the image compensation and recovery effect when the data are random missing is better than when the data are block missing because the coherence between data is damaged more seriously if the data are block missing [22]. To sum up, the algorithm in this paper is superior to the other two algorithms.

5.2 Algorithm Performance Verification under Different SNR Conditions

Considering that the sparse aperture is 50% randomly missing, the algorithm proposed in this paper is compared with the other two algorithms under different SNR conditions to illustrate its stronger robustness. Radar parameter settings are the same as above, and the experimental results are shown in Fig. 5.

Figures 5(a)–5(c) show the imaging results of three algorithms when SNR is 20 dB; Figures 5(d)–5(f) show the imaging results when SNR is 10 dB; Figures 5(g)–5(i) show the imaging results when SNR is 5 dB; Figures 5(j)–(l) show the results when SNR is 0 dB. The imaging indicators are shown in Tab. 5. As can be seen from Fig. 5, when SNR is high, 2D-JLBI and 2D-FISTA algorithms can achieve better compensation and imaging, while the 2D-SL0 algorithm is more seriously affected by noise. The imaging results of the algorithm proposed in this paper are less affected by SNR. With the decrease of SNR, 2D-FISTA and 2D-SL0 algorithms are seriously affected by noise and have poor noise suppression effects. They can no longer distinguish scattering points and noise. When SNR is 0 dB, the scattering points in the image reconstructed by them are submerged by noise, and the real scattering points and false scattering points cannot be distinguished. Table 5 shows that with the decrease of SNR, the entropy and TBR values of the imaging results of the proposed algorithm are superior to those of the other two algorithms, indicating that the proposed algorithm has stronger robustness, better noise tolerance and stronger noise suppression and it can complete translational compensation under the condition of sparse aperture.

6. Conclusion

Aiming at overcoming the difficulty in translational compensation for maneuvering targets under the condition of Bi-ISAR sparse aperture, this paper proposes a compensation and imaging method by combining 2D-JLBI reconstruction algorithm and IC search. The proposed method performs translational compensation and imaging for sparse aperture echo by establishing the compensation term of initial velocity information to carry out joint sparse reconstruction. The image with the highest quality is screened out through IC search, and the velocity information is further accurately estimated so as to obtain the optimal image circulatively. The 2D-JLBI joint sparse reconstruction method avoids the high complexity of traditional reconstruction vectorization operation and decreased coupling of range and azimuth direction in row by column processing. The method based on image maximum contrast search also ensures the accuracy of translational compensa-

tion. The simulation results show that the proposed method can still complete the compensation even when many sparse aperture data are missing. Compared with the other two algorithms, it has a stronger tolerance to noise and stronger robustness and can help to obtain higher-quality images.

Acknowledgments

This work is supported by the Natural Science Foundation of Hebei Province (no. F2019506031, F2020-506036), Basic Frontier Science and Technology Innovation Project of Army Engineering University (no. KYSZJQZL2020).

References

- [1] ZHU, X. X., SHI, L., HU, W. H., et al. Bi-ISAR sparse imaging algorithm with complex Gaussian scale mixture prior. *IET Radar, Sonar & Navigation*, 2019, vol. 13, no. 12, p. 2202–2211. DOI: 10.1049/iet-rsn.2019.0296
- [2] CABRERA, S. D., PARKS, T. W. Extrapolation and spectral estimation with iterative weighted norm modification. *IEEE Transactions on Signal Processing*, 1991, vol. 39, no. 4, p. 842–851. DOI: 10.1109/78.80906
- [3] KIM, K. T., KIM, S. W., KIM, H. T. Two-dimension ISAR imaging using full polarisation and super-resolution processing techniques. *IET Radar, Sonar and Navigation*, 1998, vol. 145, no. 4, p. 240–246. DOI: 10.1049/ip-rsn:19982033
- [4] LARSSON, E. G., LI, J., Spectral analysis of periodically gapped data. *IEEE Transactions on Aerospace and Electronic Systems*, 2003, vol. 39, no. 3, p. 1089–1097. DOI: 10.1109/TAES.2003.1238761
- [5] WANG, Y., LIU, Q. Super-resolution sparse aperture ISAR imaging of maneuvering target via the RELAX algorithm. *IEEE Sensors Journal*, 2018, vol. 18, no. 21, p. 8726–8738. DOI: 10.1109/JSEN.2018.2868308
- [6] XU, X. J., NARAYANAN, R. M., et al. Enhanced resolution in SAR/ISAR imaging using iterative sidelobe apodization. *IEEE Transactions on Image Processing*, 2005, vol. 14, no. 4, p. 537 to 547. DOI: 10.1109/tip.2004.841198
- [7] LI, S. D., CHEN, Y. B., YANG, J., et al. Imagine method with high resolution for maneuvering target based on compressive sensing. *Journal of Air Force Early Warning Academy*, 2015, vol. 29, no. 5, p. 313–321. (In Chinese)
- [8] ZHANG, S., SUN, S., ZHANG, W., et al. High-resolution bistatic ISAR image formation for high-speed and complex-motion targets. *IEEE Journal of Selected Topics in Applied Earth Observations and Remote Sensing*, 2015, vol. 8, no. 7, p. 3520–3531. DOI: 10.1109/JSTARS.2015.2417192
- [9] ZHANG, S., LIU, Y., LI, X., et al. Autofocusing for sparse aperture ISAR imaging based on joint constraint of sparsity and minimum entropy. *IEEE Journal of Selected Topics in Applied Earth Observations and Remote Sensing*, 2017, vol. 10, no. 3, p. 998–1011. DOI: 10.1109/JSTARS.2016.2598880
- [10] KANG, M., LEE, S., KIM, K., et al. Bistatic ISAR imaging and scaling of highly maneuvering target with complex motion via compressive sensing. *IEEE Transactions on Aerospace and Electronic Systems*, 2018, vol. 54, no. 6, p. 2809–2826. DOI: 10.1109/TAES.2018.2830598
- [11] LI, S. Y., ZHAO, G. Q., ZHANG, W., et al. ISAR imaging by two-dimensional convex optimization-based compressive sensing. *IEEE Sensors Journal*, 2016, vol. 16, no. 19, p. 7088–7093. DOI: 10.1109/JSEN.2016.2599540
- [12] WANG, W., HU, Z., HUANG, P. 3-D MIMO radar imaging of ship target with rotational motions. *Radioengineering*, 2019, vol. 28, no. 4, p. 776–784. DOI: 10.13164/re.2019.0776
- [13] DONOHO, D. L. Compressed sensing. *IEEE Transactions on Information Theory*, 2006, vol. 52, no. 4, p. 1289–1306. DOI: 10.1109/TIT.2006.871582
- [14] YU, T., DENG, S. J. Research of remote sensing image compression technology based on compressed sensing. In Tan, T., Ruan, Q., Wang, S., et al. (Eds.) *Advances in Image and Graphics Technologies (Proceedings of the 10th Chinese Conference IGTA)*, 2015, p. 214–223. DOI: 10.1007/978-3-662-47791-5_25
- [15] YANG, J. G., JIN, T., XIAO, C., et al. Compressed sensing radar imaging: Fundamentals, challenges, and advances. *Sensors*, 2019, vol. 19, no. 14, p. 1–19. DOI: 10.3390/s19143100
- [16] DUAN, H. P., ZHANG, L. Z., FANG, J., et al. Pattern-coupled sparse Bayesian learning for inverse synthetic aperture radar imaging. *IEEE Signal Processing Letters*, 2015, vol. 22, no. 11, p. 1995–1999. DOI: 10.1109/LSP.2015.2452412
- [17] ZHU, X. X., GUO, B. F., HU, W. H., et al. Scene segmentation of multi-band ISAR fusion imaging based on MB-PCSB. *IEEE Sensors Journal*, 2021, vol. 21, no. 3, p. 3520–3532. DOI: 10.1109/JSEN.2020.3026109
- [18] ZHANG, D., ZHANG, Y. S., FENG, C. Q., et al. Joint-2D-SL0 algorithm for joint sparse matrix reconstruction. *International Journal of Antennas and Propagation*, 2017, p. 1–7. DOI: 10.1155/2017/6862852
- [19] ZHANG, L., SHENG, J. L., DUAN, J., et al. Translational motion compensation for ISAR imaging under low SNR by minimum entropy. *EURASIP Journal on Advances in Signal Processing*, 2013, p. 1–19. DOI: 10.1186/1687-6180-2013-33
- [20] ZHANG, S. S., ZHANG, W., ZONG, Z. L., et al. High-resolution bistatic ISAR imaging based on two-dimensional compressed sensing. *IEEE Transactions on Antennas and Propagation*, 2015, vol. 63, no. 5, p. 2098–2011. DOI: 10.1109/TAP.2015.2408337
- [21] ZHU, X. X., LIU, L. M., GUO, B. F., et al. Two-dimensional multiradar ISAR fusion imaging based on fast linearized Bregman iteration algorithm. *Journal of Applied Remote Sensing*, 2021, vol. 15, no. 2, p. 1–21. DOI: 10.1117/1.JRS.15.026507
- [22] FENG, J. J., ZHANG, G. ISAR imaging based on iterative reweighted L_p block sparse reconstruction algorithm. *Progress In Electromagnetics Research M*, 2016, vol. 48, p. 155–162. DOI: 10.2528/pierm16041501

About the Authors ...

Hanshen ZHU was born in 1996. He is currently pursuing master's degree in the Department of Electronic and Optical Engineering, Shijiazhuang campus of Army Engineering University, Shijiazhuang, China. His research interests include radar signal processing and imaging technology.

Wenhua HU (corresponding author) was born in 1970. He received the Doc degree from the Department of Electronic and Optical Engineering, Shijiazhuang campus of Army Engineering University, Shijiazhuang, China in 2003.

Since 2010, he has been an Associate Professor and working here. His research interests include performance detection and fault diagnosis of radar equipment.

Baofeng GUO was born in 1987. He received the Doc degree from the Department of Electronic and Optical Engineering, Shijiazhuang campus of Army Engineering University, Shijiazhuang, China in 2015. And has been working here as a Lecturer from then on. His research interests include radar signal processing and imaging technology.

Xiaoxiu ZHU was born in 1993. She received the Ph.D. degree from the Department of Electronic and Optical Engineering, Shijiazhuang campus of Army Engineering

University, Shijiazhuang, China in 2021. Her research interests include radar imaging technology.

Dongfang XUE was born in 1983. He received the M.S degree from the Department of Electronic and Optical Engineering, Shijiazhuang campus of Army Engineering University, Shijiazhuang, China in 2010. His research interests include radar signal processing and fault diagnosis of radar equipment.

Chang'an ZHU was born in 1989. He is currently pursuing master's degree in the Department of Electronic and Optical Engineering, Shijiazhuang campus of Army Engineering University, Shijiazhuang, China. His research interests include fault diagnosis of radar equipment.

